Wang *et al. Chin. J. Mech. Eng.* (2019) 32:10
https://doi.org/10.1186/s10033-019-0325-y

Chinese Journal of Mechanical Engineering

ORIGINAL ARTICLE

Open Access

Broken Rotor Bar Fault Detection of Induction Motors Using a Joint Algorithm of Trust Region and Modified Bare-bones Particle Swarm Optimization

Panpan Wang*, Liping Shi, Yong Zhang, Yifan Wang and Li Han

Abstract

A precise detection of the fault feature parameter of motor current is a new research hotspot in the broken rotor bar (BRB) fault diagnosis of induction motors. Discrete Fourier transform (DFT) is the most popular technique in this field, owing to low computation and easy realization. However, its accuracy is often limited by the data window length, spectral leakage, fence effect, etc. Therefore, a new detection method based on a global optimization algorithm is proposed. First, a BRB fault current model and a residual error function are designed to transform the fault parameter detection problem into a nonlinear least-square problem. Because this optimization problem has a great number of local optima and needs to be resolved rapidly and accurately, a joint algorithm (called TR-MBPSO) based on a modified bare-bones particle swarm optimization (BPSO) and trust region (TR) is subsequently proposed. In the TR-MBPSO, a reinitialization strategy of inactive particle is introduced to the BPSO to enhance the swarm diversity and global search ability. Meanwhile, the TR is combined with the modified BPSO to improve convergence speed and accuracy. It also includes a global convergence analysis, whose result proves that the TR-MBPSO can converge to the global optimum with the probability of 1. Both simulations and experiments are conducted, and the results indicate that the proposed detection method not only has high accuracy of parameter estimation with short-time data window, e.g., the magnitude and frequency precision of the fault-related components reaches 10^{-4}, but also overcomes the impacts of spectral leakage and non-integer-period sampling. The proposed research provides a new BRB detection method, which has enough precision to extract the parameters of the fault feature components.

Keywords: Fault detection, Broken rotor bars, Induction motors, Bare-bones particle swarm optimization, Trust region

1 Introduction

Induction motors are widely used in the industry, owing to many advantages such as simple construction, reliability and high efficiency. Although such motors are considerably reliable and robust, they still suffer from internal machine faults caused by corrosive and dusty environments. One of the most common faults is a broken rotor bar (BRB), which accounts for approximately 10% of total induction motor faults [1]. Therefore, early BRB detection in induction motors is surely significant.

When a broken bar occurs in the rotor, the geometry and magnetic flux of the motor are unbalanced. New sideband frequency components at $(1\pm 2s)f_1$ Hz will appear in the stator current, where s is the slip and f_1 is the power supply frequency [2]. This implies that the BRB fault can be detected efficiently by using the frequencies and amplitudes of $(1\pm 2s)f_1$ components. Thus, motor current signature analysis (MCSA), which is non-invasive, is the most widely used technique for BRB detection. With MCSA, many detection methods based on

*Correspondence: wpp2011@126.com
School of Electrical and Power Engineering, China University of Mining & Technology, Xuzhou 221116, China

numerous digital signal processing techniques have been proposed in recent years.

For frequency domain analysis, the discrete Fourier transform (DFT) has been widely used in various BRB detection methods [3] to acquire signal spectrum. In fact, DFT-based methods are only efficient for stationary signals. Some drawbacks, such as spectral leakage and frequency resolution with finite-length discrete signal, limit their performance. As we know, the frequencies of fault-related components, $(1 \pm 2s)f_1$, are very close to the supply frequency and are often time-varying in a long measurement time. Meanwhile, their amplitudes are very small in the preliminary period of fault and are prone to be influenced by load level. Therefore, for DFT-based methods, a large number of data points are required to ensure enough measurement time and high frequency resolution. However, a long measurement time in which the slip and stator current remain stable is not always available. Furthermore, long measurement time will affect the accuracy of fault detection as a result of the increasing probability of load fluctuations, noise and other interference factors. To improve frequency resolution, the zoom-DFT (ZDFT) technique was introduced into BRB detection [4]. Although ZDFT increases the accuracy in a specified frequency range and lowers the calculation cost, its high-frequency resolution still requires long-time data window.

For time-frequency domain analysis, there are many signal processing techniques used in BRB fault detection, for instance, short time Fourier transform (STFT) [5], continuous/discrete wavelet transform (C/DWT) [6, 7] and wavelet packet transform (WPT) [8]. For STFT-based methods, the time-frequency resolution is restricted by the data window size. For wavelet-based techniques, a disadvantage is that the analysis result of signal is directly affected by the choice of wavelet base function and signal-to-noise ratios. Based on CWT, the generalized synchrosqueezing transform (GST), proposed by Chuanet et al. [9], is another novel time-frequency tool. It has been applied in fault detection of gearboxes [10], rolling element bearings [11] and induction motors [12]. Although its application in BRB fault detection is scarce, GST is a potential signal processing technique, especially for induction motors fed by inverters.

In other papers, the Hilbert modulus [13], product of the current and virtual flux [14] and instantaneous power [15] which are analyzed through DFT, have been used in BRB detection to avoid the problem that the characteristic components are often submerged by the fundamental component. However, these methods still require a long-time data window to obtain good frequency resolution. In Ref. [16], a new detection method was proposed based on modulation signal bispectrum (MSB) analysis. It can obtain more accurate amplitudes of the characteristic components. However, the experiment results show that the MSB-based method requires a very high sampling rate (96 kHz) and a long measurement time (20 s) to obtain sufficient MSB accuracy and frequency resolution. Another method, which combines the zooming and rotation invariance techniques, was presented in Ref. [17]. Despite of its good analysis results, the load variation is still a problem. To improve the parameter estimation accuracy of fault-related components, the high-frequency resolution spectrum analysis was combined with an optimization algorithm in Ref. [18], and experiments verified the good results of this method. Automatic identification of the BRB fault is another pressing problem. Keskesa et al. [8], and Shi et al. [19], applied a support vector machine (SVM) in BRB fault diagnosis, and the identification accuracy could meet the project requirements. However, the SVM learning efficiency is low, which limited its application. Many new machine learning methods and classifiers, such as AdaBoost [20], incremental learning [21, 22] and minimax probability machine [23], are feasible ways for addressing the above problem, but there still remains substantial research to perform before they could be actually used in induction motors.

In this paper, a new method based on a global optimization algorithm for BRB detection is proposed. At present, there are many intelligent algorithms for global optimization, such as the genetic algorithm [24], particle swarm optimization (PSO) and ant colony algorithm. Compared with other evolutionary algorithms, PSO has the advantages of simple concept, easy realization and fast convergence speed. It has been widely used in wavelet network optimization [25], impeller parameter optimization, stretch force trajectory optimization, and in other practical engineering problems. Therefore, this paper also selects it as the solver. However, when an optimization problem needs to be resolved rapidly and accurately, such as parameter estimation of the fault-related components, PSO becomes powerless. Therefore, a joint optimization algorithm, combining a modified bare-bones particle swarm optimization (BPSO) and trust region (TR), is proposed subsequently to improve the solution precision and convergence speed. The distinctive advantage of this detection method is that more accurate parameters of the fault-related components are estimated, even using a short-time data window.

2 BRB Detection Method Using Global Optimization Algorithm

For a healthy induction motor, the fundamental harmonic is a prime component, and the other harmonics are very small around the fundamental frequency. One

of the three-phase stator currents could be expressed as follows:

$$i_{\mathrm{m}}(t) = A_1 \cos(2\pi f_1 t + \phi_1), \tag{1}$$

where A_1 is amplitude of the fundamental component, f_1 is the fundamental frequency, and ϕ_1 is its phase angle.

When a BRB fault occurs, its resistance increases and causes an asymmetry in the rotor magnetic field. The asymmetry will then cause superimposed components in the stator current at $f_{brk} = (1 \pm 2ks)f_1$ Hz, where $k = 1$, 2, 3, ... Among the fault characteristic components, the amplitudes of $f_{br1} = (1 \pm 2s)f_1$ components are the maximum. Thus, the motor current of fault condition can be simulated as

$$\begin{aligned} i_{\mathrm{m}}(t) = {} & A_1 \cos(2\pi f_1 t + \phi_1) \\ & + A_2 \cos[2\pi(1-2s)f_1 t + \phi_2] \\ & + A_3 \cos[2\pi(1+2s)f_1 t + \phi_3], \end{aligned} \tag{2}$$

where $A_{2,3}$ are the amplitudes of the fault-related components, and $\phi_{2,3}$ are their phase angles.

In this section, the proposed detection method of BRB fault conducts on the current model of Eq. (2) and parameter estimation (i.e., amplitude, frequency and phase) based on a global optimization algorithm. The process is illustrated in Figure 1 and described as follows. Firstly, the actual current signal and the model current are sampled with time interval T_s, so that the data sequences of $i_s(t_i)$ and $i_m(t_i)$ can be obtained respectively, where $t_i = i \times T_s$. Then, the difference r (namely, the residual error) between $i_s(t_i)$ and $i_m(t_i)$ is calculated, which is the objective function of the optimization algorithm. The specific definition of residual error is shown as

$$r = \sum_{i=1}^{M} [i_{\mathrm{s}}(t_i) - i_{\mathrm{m}}(t_i)]^2, \tag{3}$$

where M is the sampling number.

If the residual error r is larger than the threshold, or other termination criteria are not satisfied, the optimization algorithm will produce a new set of parameters for the current model $i_m(t_i)$ by the update mechanism. The iterative process is repeated until the termination criteria are satisfied.

The objective function, Eq. (3), is a multimodal optimization problem, and has many local minimum values. For example, the projection of the residual error (in function of $2sf_1$) in Figure 2 has a lot of local minima.

For nonlinear problems, like in Eq. (3), the traditional least squares methods, such as the trust region (TR) algorithm and simplex method are powerless, because these algorithms are easily trapped into a local optimum and are very sensitive to the starting point. On the contrary, the global optimization algorithms based on population, such as PSO, are not sensitive to the starting point, and they have a strong solving ability for nonlinear problems. However, their local-search capability is poor and need to be improved.

To find the exact global optimum of Eq. (3), we select the PSO algorithm and improve it. Then, the TR is introduced to refine the result in the PSO process. The detail of the joint algorithm is described in the next section.

3 Joint Algorithm Based on Particle Swarm Optimization and Trust Region

3.1 Particle Swarm Optimization

PSO is a global, population-based optimization approach developed by Kennedy and Eberhart in 1995 [26]. With the PSO algorithm, each particle represents a candidate solution for the problem and adjusts its velocity and position based on two optima. One is its personal best position $\boldsymbol{p}_i = [p_{i1}, p_{i2}, \ldots, p_{i\alpha}]$, namely, its own flying experiences, where α is the total dimension number of search space. The other is the global best position $\boldsymbol{p}_g = [p_{g1}, p_{g2}, \ldots, p_{g\alpha}]$, namely, its companions' flying experiences. In each generation, the velocity $\boldsymbol{v}_i = [v_{i1}, v_{i2}, \ldots, v_{i\alpha}]$ and position of particle $\boldsymbol{x}_i = [x_{i1}, x_{i2}, \ldots, x_{i\alpha}]$ are updated by the following formula as [26]:

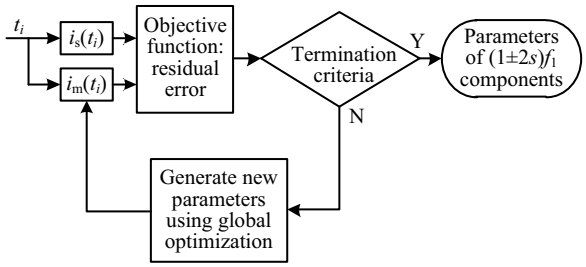

Figure 1 BRB detection method using global optimization algorithm

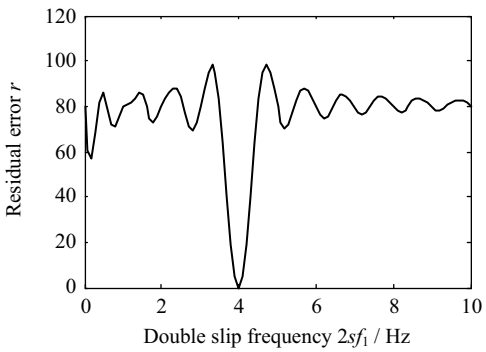

Figure 2 Residual error r in function of $2sf_1$ when the other parameters are fixed

$$v_{ij}(n+1) = \omega v_{ij}(n) + c_1 r_1 (p_{ij}(n) - x_{ij}(n)) + c_2 r_2 (p_{gj}(n) - x_{ij}(n)), \quad (4)$$

$$x_{ij}(n+1) = x_{ij}(n) + v_{ij}(n+1), \quad (5)$$

where ω is an inertia weight, c_1 and c_2 are non-negative constants, r_1 and r_2 are random numbers within [0, 1], $-v_{\max} \le v_{ij} \le v_{\max}$, and $v_{\max}$ is a maximum velocity set by the user, $i = 1, 2, \ldots, N$, N is the population size of particle swarm, $j = 1, 2, \ldots, \alpha$.

In 2003, Kennedy [27] proposed a simple PSO algorithm called bare-bones particle swarm optimization (BPSO). In BPSO, the particle's velocity, Eq. (4), is eliminated, and the position of each particle is updated by a Gaussian sampling based on $\boldsymbol{p}_i$ and $\boldsymbol{p}_g$. The updated formula is shown as

$$x_{ij}(n+1) = G\left(\mu_{ij}(n), \sigma_{ij}^2(n)\right), \quad (6)$$

where $\mu_{ij}(n) = (p_{ij}(n) + p_{gj}(n))/2$ and $\sigma_{ij}^2(n) = |p_{ij}(n) - p_{gj}(n)|$ are the mean and standard deviation of the Gaussian distribution, respectively. Unlike the canonical PSO, BPSO is obviously control-parameter-free and more suitable for practical engineering problems.

3.2 Modified BPSO

BPSO is a global optimal algorithm but it still easily falls into a local optimum [27]. With the increasing number of iterations, particles will gather around the global best particle. The distance between $\boldsymbol{p}_i$ and $\boldsymbol{p}_g$ decrease significantly, which makes the probability that the particle moves to a new position very small. If the global best particle is a local optimum of the optimized problem, it is difficult to escape from this local optimum. Aiming at this problem, a reinitialization strategy of the inactive particle is introduced into the BPSO to enhance the swarm diversity and global search ability. The definition of the inactive particle is as follows.

Definition 1 For a particle, if its fitness is no improvement for η cumulative iterations, we will consider it as an inactive particle, where η is the inactive coefficient.

To record the change of particles, a parameter ***stagnation_iteration*** is used to monitor the fitness value for each particle. At each iteration, if there is no fitness improvement for a particle $\boldsymbol{x}_i$, the ***stagnation_iteration***$[i]$ will be increased by one, or else, decreased by one. If ***stagnation_iteration*** $[i] \ge \eta$, this particle will be seen as inactive particle, and then be reinitialized. Meanwhile, the inactive particle will forget its memory and select the current position to be the personal best position. This reinitialization operator will help the inactive particle escape from the local optimum and improve its search efficiency. The inactive coefficient η, set by the user according to the problem complexity, adjusts the number of the initialized particle to make the MBPSO achieve a satisfactory balance of exploitation and exploration capability.

3.3 Trust Region Algorithm

TR is a popular iterative algorithm used for solving unconstrained optimization problems [28]. It is based on the Newton's method and has strong convergence and stability. In the implementation process, a starting point $\boldsymbol{x_0}$ and trust region radius r_0 need to be given at first. Then, according to the iterative rules, a sequence of points $\{\boldsymbol{x}_k\}$ is generated to search for the optimal solution. At each iteration, the TR iterative mechanism is as follows. Firstly, a small region is initialized as a trust region centering on the current iteration point, and a trial step $\boldsymbol{d}_k$ is calculated by solving a sub-problem within this region. Then, an evaluation function is used to decide whether to accept the trial step and determine the trust region radius of next iteration. If the trial step is accepted, $\boldsymbol{x}_{k+1} = \boldsymbol{x}_k + \boldsymbol{d}_k$, otherwise, $\boldsymbol{x}_{k+1} = \boldsymbol{x}_k$. The new radius of the trust region depends on the trial step quality. In general, if the trial step is suitable, the new radius will be expanded or maintained. Otherwise, it will be reduced.

Because the TR makes full use of the problem's information and region knowledge, it has fast convergence speed and strong local searching ability. However, for multimodal and multivariate optimization problems, it often traps in local optima and is difficult to obtain the global optimal point. This is because the next search direction of TR is only based on the local develop ability of objective function.

3.4 Joint Algorithm Based on MBPSO and TR

To improve the convergence speed and avoid "premature convergence" at the late stage of PSO algorithm, TR is introduced into MBPSO. In the iteration process of MBPSO, TR is applied to the global best particle every K iterations. This combining strategy not only makes use of the experience and information of particle swarm, but also considers the computational cost of TR, which makes the joint algorithm (called TR-MBPSO) achieve fast and efficient convergence performance with a small amount of computational cost. In addition, according to the problem's complexity, this strategy can adjust the call frequency of trust-region search to improve the quality of solution and search efficiency.

The key steps of TR-MBPSO are outlined as follows.

Step 1: Initialization. Initialize all particles, personal best positions, global best position and ***stagnation_iteration***, set the parameters, such as size of swarm N,

maximum generation $m_{\max}$, interval generation K and inactive coefficient η.

Step 2: Calculate each particle's fitness.

Step 3: Update each personal best position, according to

$$\begin{cases} \boldsymbol{p_q}(n+1) = \boldsymbol{x_q}(n+1), \\ \boldsymbol{p_i}(n+1) = \begin{cases} \boldsymbol{p_i}(n) & fit(\boldsymbol{p_i}(n)) \le fit(\boldsymbol{x_i}(n+1)) \\ \boldsymbol{x_i}(n+1) & fit(\boldsymbol{p_i}(n)) > fit(\boldsymbol{x_i}(n+1)) \end{cases} (i \ne q), \end{cases} \tag{7}$$

where $fit(\cdot)$ is the fitness function, $\boldsymbol{p}_q$ is the personal best position of inactive particle, and $\boldsymbol{p}_i$ is the personal best position of the other particle.

Step 4: Reinitialize ***stagnation_iteration***$[q]$ of inactive particles. For the remaining particles, if their fitness does not change, the ***stagnation_iteration***$[i]$ will be increased by 1, or else, decreased by 1.

Step 5: Update the global best position $\boldsymbol{p}_{\mathrm{g}}$.

Step 6: If $n/K = \lfloor n/K \rfloor$ (where $\lfloor \cdot \rfloor$ indicates rounding down), apply TR to the global best particle and update.

Step 7: Update each particle position. If the particle is an inactive particle, reinitialize its position at random; otherwise, update the position according to Eq. (6).

Step 8: If the termination criteria are satisfied, stop the iteration procedure and output the optimal solution; otherwise, go to step 2.

3.5 Global Convergence Analysis

In Ref. [29], Solis and Wets have discussed the convergence of stochastic search algorithms. For convenience, the relevant definitions are shown below again.

Lemma 1 $fit(F(\boldsymbol{p}_{\mathrm{g}}, \boldsymbol{\xi})) \le fit(\boldsymbol{p}_{\mathrm{g}})$ and if $\boldsymbol{\xi} \in \mathbf{S}$, then $fit(F(\boldsymbol{p}_{\mathrm{g}}, \boldsymbol{\xi})) \le fit(\boldsymbol{\xi})$.

Where F is a function that constructs a solution to the problem, $\boldsymbol{\xi}$ is a vector generated from the sample space $(\mathbf{R}^{\alpha}, \mathbf{B}, \mu_n)$, the search space $\mathbf{S}$ is a subset of $\mathbf{R}^{\alpha}$, μ_t is a probability measure on $\mathbf{B}$, and $\mathbf{B}$ is the σ-algebra of a subset of $\mathbf{R}^{\alpha}$.

This means that the solution suggested by F carries the guarantee that the newly constructed solution will be no worse than the current solution. Different F functions lead to different algorithms, but condition **Lemma 1** must be satisfied for an optimization algorithm to work correctly.

Lemma 2 For any Borel subset $\mathbf{A}$ of $\mathbf{S}$ with $\Theta[\mathbf{A}] > 0$, we have that

$$\prod_{n=0}^{\infty} (1 - \mu_n(\mathbf{A})) = 0, \tag{8}$$

where $\Theta[\mathbf{A}]$ is the Lebesgue measure, and $\mu_n(\mathbf{A})$ is the probability of $\mathbf{A}$ being generated by μ_n.

This means that for any subset $\mathbf{A}$ of $\mathbf{S}$ with positive measure Θ, the probability of repeatedly missing the set $\mathbf{A}$ using random samples (e.g., the $\boldsymbol{\xi}$ above), must be zero.

Theorem 1 Suppose that $fit(\cdot)$ is a measurable function, $\mathbf{S}$ is a measurable subnet of $\mathbf{R}^{\alpha}$, and **Lemma 1** and **Lemma 2** are satisfied. $\{\boldsymbol{p}_{\mathbf{g}}(n)\}_{n=0}^{\infty}$ is a sequence generated by the algorithm. Then,

$$\lim_{n \to +\infty} P(\boldsymbol{p}_{\mathbf{g}}(n) \in \mathbf{R}_{\varepsilon}) = 1, \tag{9}$$

where $\mathbf{R}_{\varepsilon}$ is the optimality region, $P(\boldsymbol{p}_{\boldsymbol{g}}(n) \in \mathbf{R}_{\varepsilon})$ is the probability that at step n, the point $\boldsymbol{p}_{\mathbf{g}}(n)$ generated by the algorithm is in $\mathbf{R}_{\varepsilon}$. By **Theorem 1**, we thus have that an algorithm satisfying **Lemma 1** and **Lemma 2** is a global optimization algorithm.

Because the TR-MBPSO belongs to the framework of a global stochastic search algorithm, its convergence can be proved by **Theorem 1**. Therefore, we only need to validate that the TR-MBPSO satisfies both **Lemma 1** and **Lemma 2**.

Suppose that $\{\boldsymbol{p}_{\mathrm{g}}(n)\}$ is a sequence generated by the TR-MBPSO algorithm, where $\boldsymbol{p}_{\mathrm{g}}(n)$ is the current best position of the swarm at time n, and function F is defined as

$$F(\boldsymbol{p}_{\mathbf{g}}(n), \boldsymbol{x_i}(n)) = \begin{cases} \boldsymbol{p}_{\mathbf{g}}(n), & fit(\boldsymbol{p}_{\mathbf{g}}(n)) \le fit(\boldsymbol{x_i}(n)), \\ \boldsymbol{x_i}(n), & fit(\boldsymbol{p}_{\mathbf{g}}(n)) > fit(\boldsymbol{x_i}(n)). \end{cases} \tag{10}$$

According to Eq. (10), the TR-MBPSO clearly satisfies **Lemma 1** because the sequence $\boldsymbol{p}_{\mathrm{g}}(n)$ is monotonic by definition.

If the TR-MBPSO algorithm satisfies **Lemma 2**, the union of the sample spaces of the particles must cover $\mathbf{S}$, i.e.,

$$\mathbf{S} \subseteq \bigcup_{i=1}^{N} \mathbf{M}_{i,n}, \tag{11}$$

where $\mathbf{M}_{i,n}$ denotes the support of the sample space of particle i at time step n, and N is the population size.

Because the inactive particles re-initialize their positions in the whole search space in TR-MBPSO, the support sets of these sample spaces $\mathbf{M}_{q,n}$, are equal to the whole search space. This means $\Theta[\mathbf{M}_{q,n}] = \Theta[\mathbf{S}]$. Thus, the TR-MBPSO algorithm satisfies **Lemma 2**.

According to **Theorem 1**, the TR-MBPSO must be a global search algorithm.

4 Detection Procedure of TR-MBPSO-Based Method and Simulation Analysis

4.1 Procedure

Based on Sections 2 and 3.4, the key steps of the proposed detection method are as follows.

Step 1: Measure the stator current $i_s(t_i)$.

Step 2: Initialize all the particles which are coded as $\boldsymbol{x_i} = (A_1, f_1, \phi_1, A_2, 2sf_1, \phi_2, A_3, \phi_3)$, their personal best positions, global best position and ***stagnation_iteration***; set the parameters, such as size of swarm N, maximum generation $m_{\max}$, interval generation K and inactive coefficient η.

Step 3: Calculate each particle's fitness by using Eq. (3).

Step 4: Update each personal best position, according to Eq. (7).

Step 5: Reinitialize ***stagnation_iteration***$[q]$ of inactive particles. For the remaining particles, if their fitness does not change, the ***stagnation_iteration***$[i]$ will be increased by 1, or else, decreased by 1.

Step 6: Update the global best position $\boldsymbol{p}_g$.

Step 7: If $n/K = \lfloor n/K \rfloor$, apply TR to the global best particle and update.

Step 8: Update each particle position. If the particle is an inactive particle, reinitialize its position at random; otherwise, update the position according to Eq. (6).

Step 9: If the termination criteria are satisfied, stop the iteration procedure, and output the optimal solution, i.e., the parameters of the fundamental and fault-related components; otherwise, go to Step 3.

4.2 Simulation Analysis

To analyze the performance of the proposed detection method, a simulated signal is designed as BRB-fault stator current, that is

$$\begin{aligned} i_s(t) = {} & 10\cos(100\pi t - \pi/4) \\ & + 0.2\cos[2\pi(50 - 0.4)t + \pi/2] \\ & + 0.2\cos[2\pi(50 + 0.4)t + \pi]. \end{aligned} \tag{12}$$

In this simulation, the sampling rate is 1000 Hz, and the sampling number of per signal rises at different samples, such as 1000, 2000, 3000 and 4000.

Firstly, the proposed detection method is tested with 1000 data samples (i.e., the length of data window is only 1 s). Both BPSO and TR-MBPSO are selected to solve the parameter-estimation problem for comparison, and their parameter configurations are summarized in Table 1.

To compare the optimal ability and convergence speed, the performance of the TR-MBPSO is compared with BPSO based on BV, MV, WV, and SR, where BV, MV and WV are the best value, mean value and worst value of the residual error, respectively. It is clear that the fitness value of the known global optimum is 0 in this problem, and the optimal solution is (10, 50, −π/4, 0.2, 0.4, π/2, 0.2, π). SR is the success rate of optimization. In the simulation process, a run is considered successful if its result is close to the known global optimum within 0.1. Because PSO is a stochastic optimization algorithm, all the results of the metrics, which are summarized in Table 2, are averaged over 30 runs.

The BV and MV of the TR-MBPSO are much better than those of the BPSO, which indicates that the proposed algorithm has a more powerful search capability. In addition, the smaller WV value indicates its better stabilization. Because of the reinitialization strategy of the inactive particle, the TR-MBPSO has higher probability of finding the global optimal value. As Table 2 shown, the TR-MBPSO is capable of converging to the global optimum with 100% successful rate, while the BPSO's SR is only 13.3%, which means that the robustness of the proposed algorithm is strong enough to solve the BRB detection problem.

Figure 3 graphically presents the convergence characteristics of the algorithms' evolutionary processes in solving the parameter estimation problem. From Figure 3, we find that the TR-MBPSO converges to the near-optimal solution faster than the BPSO and can get a better solution at the end of evolution process.

For BRB fault detection, the solution quality is more important because it contains amplitude, frequency and phase of the fault-related components. Table 3 shows the parameter estimation results of the proposed detection method, while Table 4 shows the estimation error comparison using different optimization algorithms. All the results are statistical data based on 30 runs.

Although the BPSO-based method has good estimation of the fundamental-component parameters, the

Table 1 Parameter configurations for selected optimization algorithms

Parameter	BPSO	TR-MBPSO
Population size N	50	50
Maximum generation $m_{\max}$	80	80
Inactive coefficient η	–	10
Interval generation K	–	20

Table 2 Optimal performance comparison of the selected algorithms

Algorithm	Index			
	BV	MV	WV	SR
BPSO	2.912×10^{-3}	3.594×10^{-1}	1.519	0.133
TR-MBPSO	1.872×10^{-23}	2.769×10^{-5}	8.272×10^{-4}	1

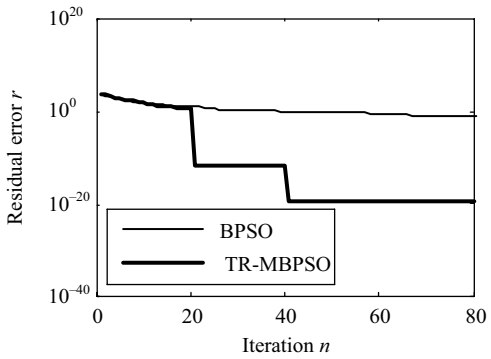

Figure 3 Fitness evolutionary curves

estimation accuracy of the fault-related parameters is not high enough so that the reliability of the BRB fault detection is affected. On contrast, all the parameters of the fundamental component and fault-related components are determined accurately by the TR-MBPSO-based method, even with a short-time data window. The error data shown in Table 4 further validates the superiority of the proposed detection method in parameter estimation accuracy. Amplitude and frequency of the fault-related components are the key parameters for BRB fault detection. As shown in Table 4, the estimation precision of these two parameters reaches 10^{-4}. Under the worst condition, the max error will not exceed 10^{-3}. Therefore, the TR-MBPSO-based detection method is sensitive enough for the BRB indicator.

Figure 4 graphically displays the spectrum analysis results of the proposed method and DFT. Because the frequency interval between the fundamental and fault-related components is only 0.4 Hz, the data-window length of the DFT method must be extended. Thus, different-length data windows, such as 2, 3 and 4 s, are selected to apply in the DFT method, and the results are shown in Figure 4(b)–(d), and Table 5. From Figure 4(b), no spectrum peaks of the fault-related components are found; therefore, their amplitudes, frequencies, and phases are also not acquired, causing a final failure of BRB detection. In Figure 4c, its frequency resolution, 0.33 Hz, is less than the frequency interval between fundamental and fault-related components. However, the fault characteristics cannot be identified owing to spectral leakage from the fundamental component. Although the frequency resolution of Figure 4(d), 0.25 Hz, is enough to identify the characteristics, the fault-related components are not very clear because of spectral leakage and non-integer-period sampling. Compared with Figure 4(b)–(d), the proposed method has such a high frequency resolution that the characteristics of the fault components can be clearly identified, and eliminates the influence of spectral leakage and non-integer-period sampling.

Table 5 presents the DFT estimation results, which are computed with different-length data windows. Because the lengths of the three data windows are integer times of the fundamental period, the DFT method gets good results regarding amplitude and frequency of the fundamental component. However, an obvious deviation occurs in phase estimation. For the DFT estimation computed with data window length of 2 or 3 s, the parameters of fault-related components are still unavailable owing to identification failure of characteristic peaks in Figure 4(b), (c). The DFT estimation computed with data-window length of 4 s is able to obtain all parameters of

Table 3 Estimation results of the proposed detection method using different optimization algorithms

Parameter	True value	Average estimation value based on BPSO	Average estimation value based on TR-MBPSO
Amplitude A_1 (A)	10	10.0722	9.9998
Frequency f_1 (Hz)	50	50.0035	50.0000
Phase φ_1 (rad)	$-\pi/4$	−0.7971	−0.7854
Amplitude A_2 (A)	0.2	0.2176	0.2002
Frequency $2sf_1$ (Hz)	0.4	0.4849	0.3997
Phase φ_2 (rad)	$\pi/2$	1.8847	1.5683
Amplitude A_3 (A)	0.2	0.1927	0.1999
Phase φ_3 (rad)	π	2.4169	3.1416

Table 4 Estimation error comparison using different optimization algorithms

Parameter	BBPSO		TR-MBPSO	
	Mean error	Max error	Mean error	Max error
Amplitude A_1 (A)	7.284×10^{-2}	2.385×10^{-1}	2.826×10^{-4}	7.915×10^{-4}
Frequency f_1 (Hz)	7.353×10^{-3}	2.303×10^{-2}	2.097×10^{-5}	5.891×10^{-4}
Phase φ_1 (rad)	2.427×10^{-2}	7.638×10^{-2}	6.765×10^{-5}	1.894×10^{-3}
Amplitude A_2 (A)	6.675×10^{-2}	1.996×10^{-1}	2.962×10^{-4}	8.240×10^{-3}
Frequency $2sf_1$ (Hz)	9.642×10^{-2}	1.987×10^{-1}	3.243×10^{-4}	9.123×10^{-3}
Phase φ_2 (rad)	5.703×10^{-1}	1.537	2.857×10^{-3}	8.045×10^{-2}
Amplitude A_3 (A)	3.514×10^{-2}	9.422×10^{-2}	7.625×10^{-6}	2.123×10^{-4}
Phase φ_3 (rad)	7.247×10^{-1}	1.890	2.238×10^{-7}	3.356×10^{-6}

the fault-related components, while its estimation accuracy is low, especially in amplitude and phase estimation. The reason is that the data length is not integer times of the period of fault-related components.

From Table 5 and Figure 4, it can be seen that the DFT method needs a longer data window to guarantee detection performance and estimation accuracy. However, a long measurement time would increase the probability of load variation and noise influence, and then decrease the reliability of fault detection.

The aforementioned analysis reveals that the proposed method has very significant advantages in terms of using a much shorter data window to satisfy high-precision detection of fault feature parameter, compared with the DFT technique. Therefore, the reasonable conclusion can be drawn that the proposed method is practical to detect a BRB fault and is preferable for motors with small slip and fluctuant load, as only a short-time measurement is required.

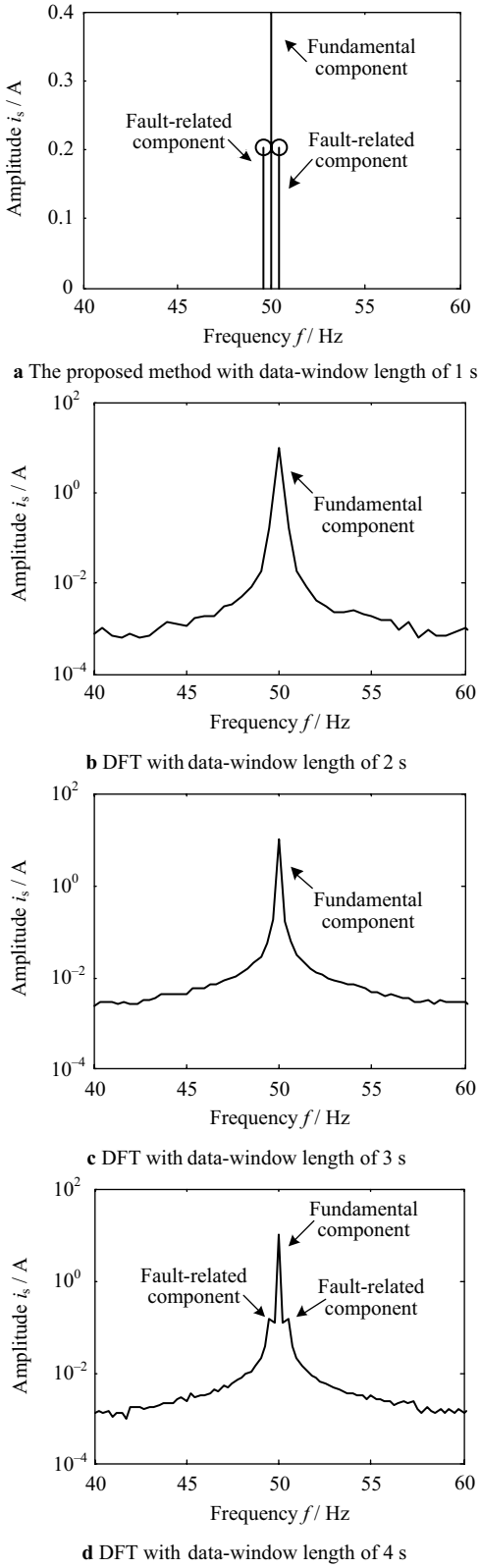

Figure 4 Simulated current spectrum with different detection method

5 Experimental Verification

5.1 Experimental Setup

Figure 5 presents the overview of the induction motor experimental system. The motor drives an 8 kW generator to supply 20 sets of incandescent bulbs. The incandescent bulb groups can be switched to adjust the motor load as required.

The type of test motor is Y132 M-4, and its specifications are shown in Table 6. Besides a healthy rotor, the motor is equipped with a fault rotor, which has one broken bar. Three Hall current sensors LAH25-NP are equipped for motor-current measurement. The discrete current data is acquired into the computer for detection and analysis by the analog signal acquisition card

Table 5 DFT estimation results with different lengths of data window

Parameter	True value	Different lengths of data window		
		2 s	3 s	4 s
Amplitude A_1 (A)	10	10.0917	9.9904	10.0677
Frequency f_1 (Hz)	50	50.000	50.000	50.000
Phase φ_1 (rad)	$-\pi/4$	−2.3562	−2.3562	−2.3562
Amplitude A_2 (A)	0.2	—	—	0.1417
Frequency $2sf_1$ (Hz)	0.4	—	—	0.5000
Phase φ_2 (rad)	$\pi/2$	—	—	1.3516
Amplitude A_3 (A)	0.2	—	—	0.1423
Phase φ_3 (rad)	π	—	—	2.7031

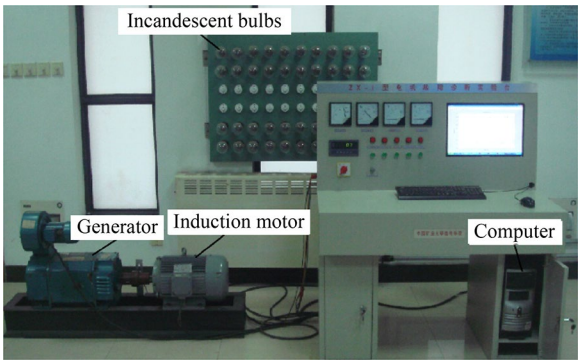

Figure 5 Experimental setup

Table 6 Specifications of the test motor

Rated power P_N (kW)	Rated voltage U_N (V)	Rated current I_N (A)	Rated speed n_N (r/min)	Number of rotor bars
7.5	380	15.4	1440	32

PCI8622. The detection tests were performed with the equipment described above, first using a healthy motor, then a motor with one broken bar. In each case, three different levels of load were used: full, medium and low. The signal-sampling period is 0.7 ms, and the sampling number of per signal rises at 13,000 samples.

During the experiments, one phase stator current with 2000 samples (i.e., the data-window length is 1.4 s) was analyzed by the DFT method and the proposed method respectively. Meanwhile, 13,000 signal samples (i.e., the data-window length is 9.1 s) were also used with the DFT method for comparison. The parameter configurations of TR-MBPSO are the same as in Table 1.

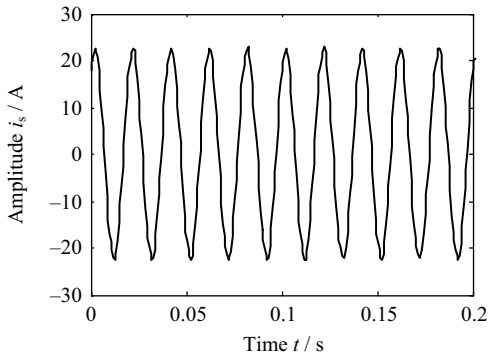

a Stator current

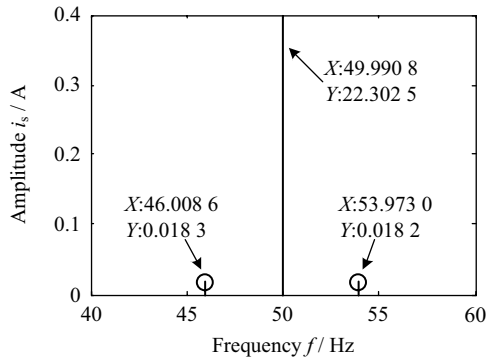

b The proposed method with data-window length of 1.4 s

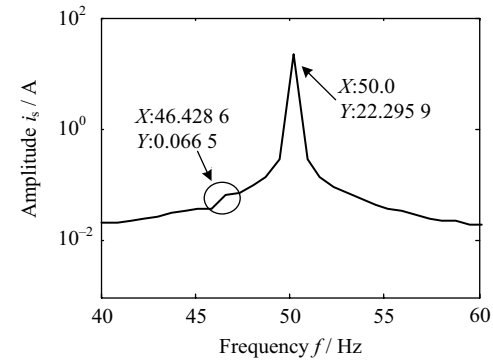

c DFT with data-window length of 1.4 s

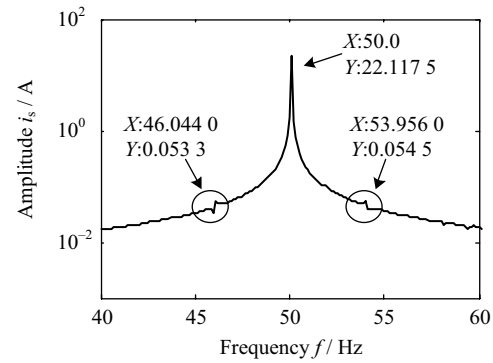

d DFT with data-window length of 9.1 s

Figure 6 Healthy and full-load case: stator current and spectrum analysis results with different detection methods

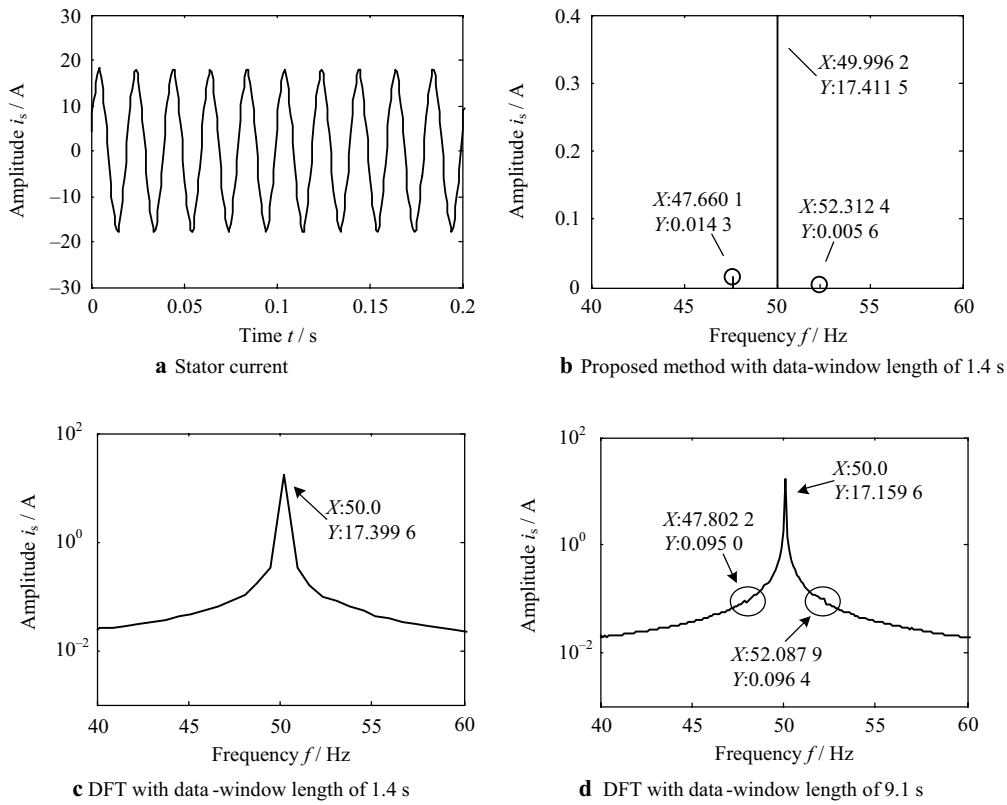

a Stator current

b Proposed method with data-window length of 1.4 s

c DFT with data -window length of 1.4 s

d DFT with data -window length of 9.1 s

Figure 7 Healthy and medium-load case: stator current and spectrum analysis results with different detection methods

5.2 Experimental Results

Under the healthy condition, Figures 6, 7 and 8 show the stator current and spectra analyzed by the proposed method and DFT, respectively. For comparison, Figures 9, 10 and 11 provide the corresponding results under faulty condition.

For the healthy motor operating with medium and low load, the DFT-analysis results based on two different data lengths are consistent with the reality, as shown in Figures 7(c), (d) and 8(c), (d). However, the DFT method cannot obtain satisfactory results when the motor is fully loaded. As shown in Figure 6(d), although the motor is healthy, the DFT spectrum computed with data-window length of 9.1 s has two peaks at 46.0440 Hz and 53.9560 Hz, which are close to $(1-2\,s)f_1$ ($\approx$45.9253 Hz) or $(1+2\,s)f_1$ ($\approx$54.0587 Hz), and their amplitudes are both greater than 0.05. In Figure 6(c), the DFT spectrum computed with data-window length of 1.4 s also has a peak at 46.4286 Hz. Hence, it is likely that those peaks could be misinterpreted as the BRB indicator, leading to a false diagnosis.

Although Figures 6(b), 7(b) and 8(b), which are the spectrum analysis results of the proposed method, also have peaks around the fault-related frequency, their amplitudes are very small (less than 0.02). Compared with the faulty condition, as shown in Figures 9(b), 10(b) and 11(b), the amplitudes are small enough. Therefore, it eliminates the possibility of false diagnosis.

In addition, under different load conditions, the actual frequency values of the fundamental component are 49.9920 Hz, 49.9637 Hz and 50.0048 Hz, respectively. In Figures 6, 7 and 8, it is clear that the proposed method has higher accuracy in frequency estimation. The DFT method also achieves a good precision, but it can only present the peaks at the integer multiples of the frequency resolution, which limits the estimation precision.

When the motor load is mediumor full, the two methods can distinguish fault-related components, as shown in Figures 9 and 10. However, the distinction effects of the proposed method are more obvious. This is because its calculation principles can effectively avoid the spectrum leakage and fence effect. It is clear that the proposed method has best performance; the DFT analysis computed with data-window length of 9.1 s ranks second, and the DFT analysis computed with data-window length of 1.4 s obtains the worst performance. These results demonstrate that the TR-MBPSO-based method is practical to detect a BRB fault using a short-time data window.

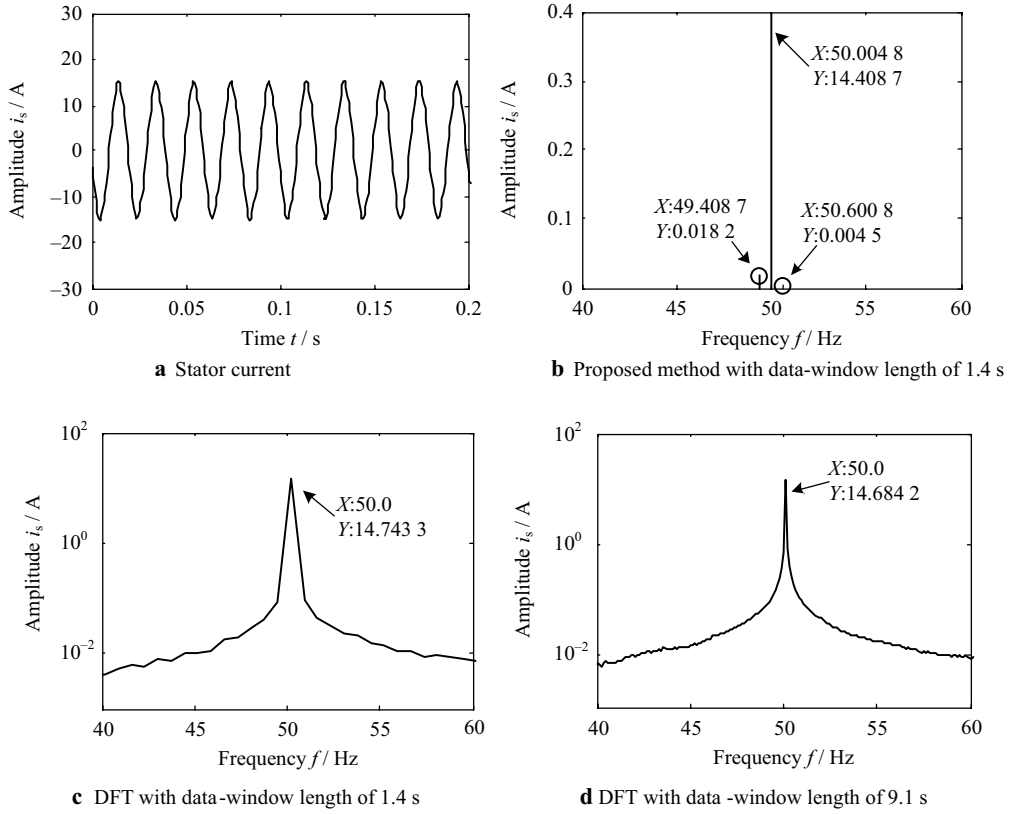

a Stator current

b Proposed method with data-window length of 1.4 s

c DFT with data-window length of 1.4 s

d DFT with data -window length of 9.1 s

Figure 8 Healthy and low-load case: stator current and spectrum analysis results with different detection methods

Under the low-load case, the proposed method and the DFT analysis computed with data-window length of 9.1 s can successfully identify the fault characteristic, as shown in Figure 11. However, the DFT spectrum computed with data-window length of 1.4 s is not satisfactory. From Figure 11(c), we can see that the sideband components are submerged completely by the fundamental component. The reason is that the frequency resolution of the 1.4 s data window is 0.7143 Hz, while the frequency interval between the characteristic and fundamental components is only 0.67 Hz.

On the contrary, Figure 11(b) shows that the spectrum of the proposed method can present the BRB indicator at more precise frequencies (realistic $(1-2\ s)f_1$ ($\approx$49.3400 Hz) and $(1+2\ s)f_1$ ($\approx$50.6734 Hz)). Thus, it is easier to determine a BRB fault using these frequency values. Further, this also demonstrates that the proposed method can achieve a high-frequency resolution even with a short-time data window.

Comparing Figures 6, 7 and 8 with Figures 9, 10 and 11, it is easy to conclude that the proposed method is very sensitive and adequate for BRB detection in induction motors operating with different loads, even when the motors are in the incipient fault stage (with one BRB).

6 Conclusions

1) Based on a BRB fault current model and residual error function, a novel BRB detection method using a global optimization algorithm is proposed. The simulation results show that, compared with DFT, it has higher detection precision of the fault feature parameter even with a short data window, no spectral leakage, and without integer-period sampling.
2) A joint algorithm TR-MBPSO is proposed by combining a modified BPSO and the TR. Compared with the BPSO, the TR-MBPSO makes good use of the characteristics of the two algorithms, and obtains a noticeable improvement in solution quality, convergence rate and robustness.
3) The theory analysis of algorithm convergence is implemented. The results show that the TR-MBPSO can converge to the global optimum with the probability of 1.

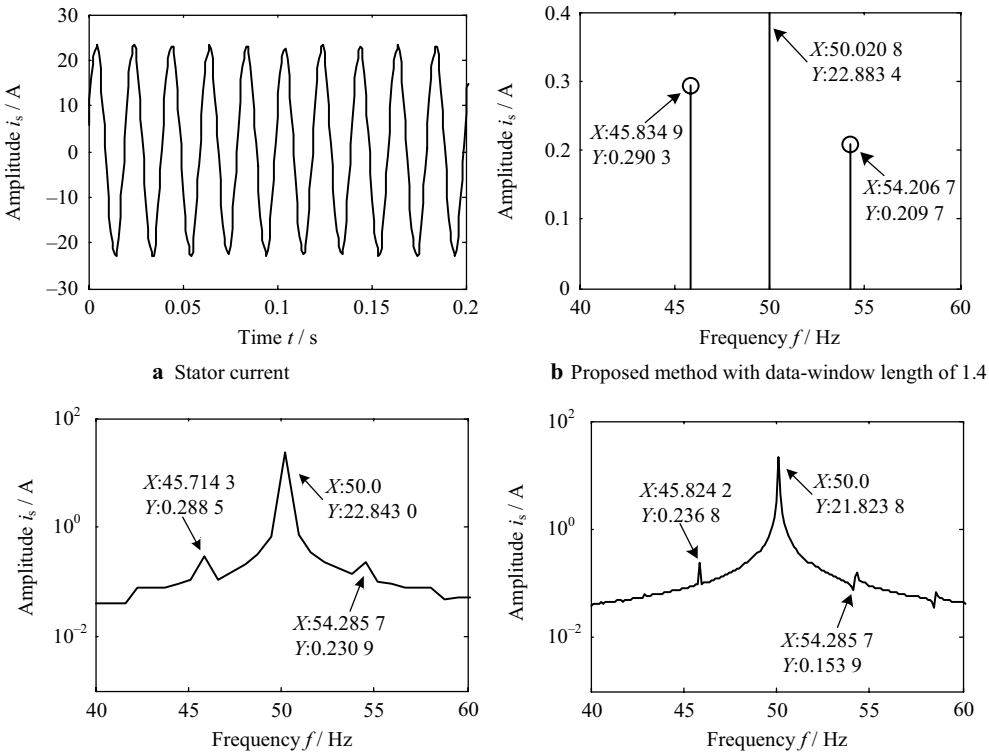

a Stator current

b Proposed method with data-window length of 1.4 s

c DFT with data-window length of 1.4 s

d DFT with data -window length of 9.1 s

Figure 9 Fault and full-load case: stator current and spectrum analysis results with different detection methods

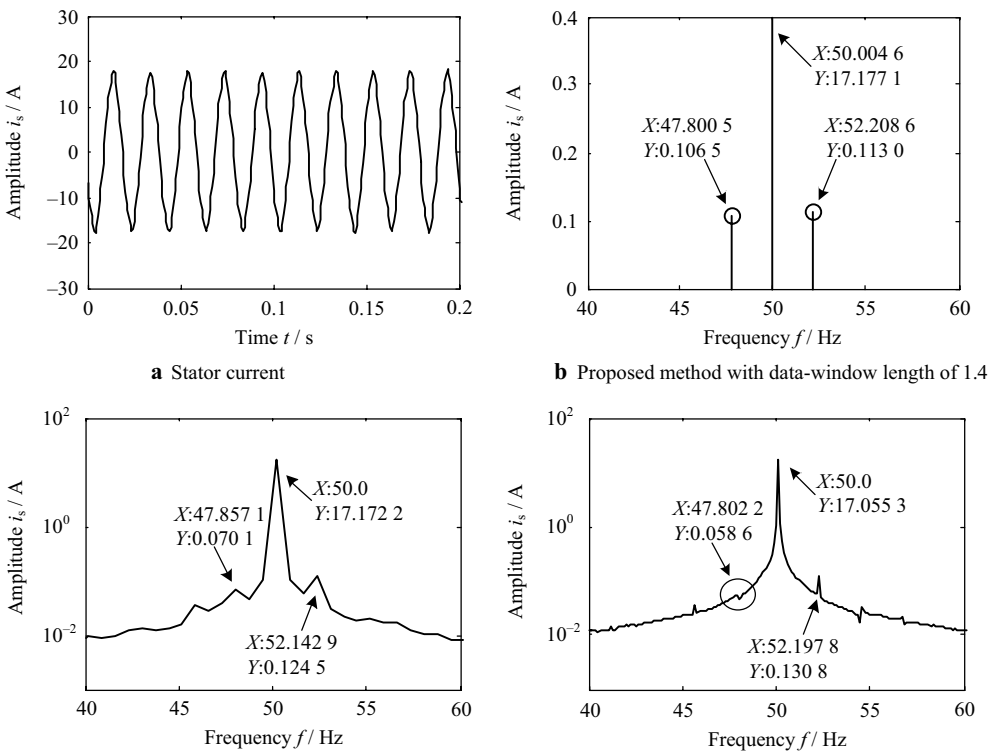

a Stator current

b Proposed method with data-window length of 1.4 s

c DFT with data -window length of 1.4 s

d DFT with data -window length of 9.1 s

Figure 10 Fault and medium-load case: stator current and spectrum analysis results with different detection methods

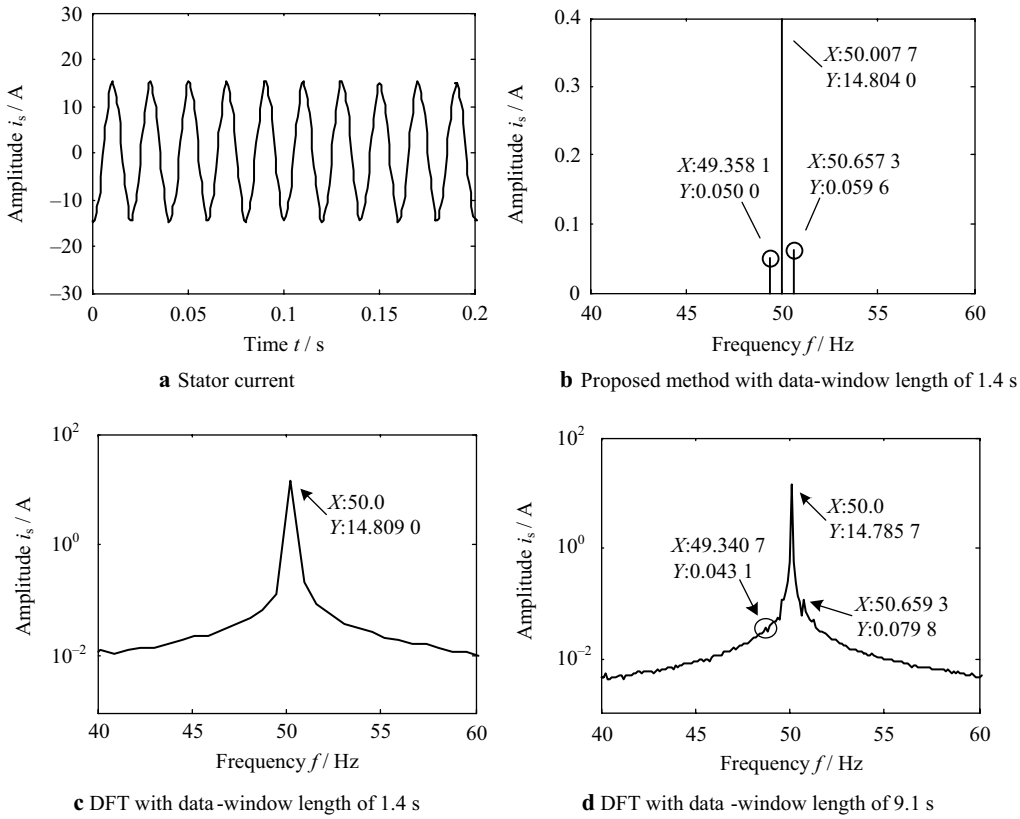

a Stator current

b Proposed method with data-window length of 1.4 s

c DFT with data-window length of 1.4 s

d DFT with data -window length of 9.1 s

Figure 11 Fault and low-load case: stator current and spectrum analysis results with different detection methods

4) Finally, experiments on a real induction motor are implemented. The results verify the feasibility and superiority of the proposed detection method.

Authors' Contributions

PW was in charge of the whole trial; PW, LS and YZ wrote the manuscript; YW and LH assisted with sampling and laboratory analyses. All authors read and approved the final manuscript.

Authors' Information

Panpan Wang, born in 1982, is currently a lecturer at *China University of Mining & Technology, China*. He received his PhD degree from *China University of Mining & Technology, China*, in 2013. His research interests include fault diagnosis of induction motor, intelligence optimization and signal processing.

Liping Shi, born in 1964, is currently a professor at *China University of Mining & Technology, China*. She received his PhD degree from *China University of Mining & Technology, China*, in 2001. Her research interests include intelligence optimization, fault diagnosis and artificial intelligence.

Yong Zhang, born in 1979, is currently an associate professor at *China University of Mining & Technology, China*. He received his PhD degree from *China University of Mining & Technology, China*, in 2009. His research interests include intelligence optimization and control.

Yifan Wang, born in 1993, is currently a master candidate at *China University of Mining & Technology, China*.

Li Han, born in 1977, is currently an associate professor at *China University of Mining & Technology, China*. She received his PhD degree from *Southeast University, China*, in 2005. Her research interests include wind power forecast and fault diagnosis.

Competing Interests

The authors declare that they have no competing interests.

Funding

Supported by Fundamental Research Funds for the Central Universities (Grant No. 2017XKQY032).

Publisher's Note

Received: 5 May 2018 Accepted: 28 January 2019
Published online: 18 February 2019

References

[1] S Bindu, V V Thomas. Diagnoses of internal faults of three phase squirrel cage induction motor – A review. *Proceedings of the IEEE International Conference on Advances in Energy Conversion Technologies*, Manipal, India, January 23–25, 2014: 48–54.

[2] V Ghorbanian, J Faiz. A survey on time and frequency characteristics of induction motors with broken rotor bars in line-start and inverter-fed modes. *Mechanical Systems and Signal Process*, 2015, 54(1): 427–456.

[3] M R Mehrjou, N Mariun, M H Marhaban, et al. Rotor fault condition monitoring techniques for squirrel-cage induction machine – A review. *Mechanical Systems and Signal Process*, 2011, 25(8): 2827–2848.

[4] A Bellini, A Yazidi, F Filippetti, et al. High frequency resolution techniques for rotor fault detection of induction machines. *IEEE Transactions on Industrial Electronics*, 2008, 55(12): 4200–4209.

[5] A F Aimer, A H Boudinar, N Benouzza, et al. Simulatioin and experimental study of induction motor broken rotor bars fault diagnosis using stator current spectrogram. *Proceedings of the IEEE International Conference on Control, Engineering and Information Technology*, Tlemcen, Algeria, May 25–27, 2015: 1–7.
[6] M Pineda-Sanchez, M Riera-Guasp, J Perez-Cruz, et al. Transient motor current signature analysis via modulus of the continuous complex wavelet: a pattern approach. *Energy Conversion & Management*, 2013, 73(5): 26–36.
[7] P Karvelis, G Georgoulas, I P Tsoumas, et al. A symbolic representation approach for the diagnosis of broken rotor bars in induction motors. *IEEE Transactions on Industrial Informatics*, 2015, 11(5): 1028–1037.
[8] H Keskesa, A Brahama, Z Lachiri. Broken rotor bar diagnosis in induction machines through stationary wavelet packet transform and multiclass wavelet SVM. *Electric Power Systems Research*, 2013, 97(2): 151–157.
[9] C Li, M Liang. A generalized synchrosqueezing transform for enhancing signal time-frequency representation. *Signal Processing*, 2012, 92(9): 2264–2274.
[10] Z Feng, X Chen, M Liang. Iterative generalized synchrosqueezing transform for fault diagnosis of wind turbine planetary gearbox under nonstationary conditions. *Mechanical Systems and Signal Processing*, 2015, 52(1): 360–375.
[11] C Li, V Sanchez, G Zutita, et al. Rolling element bearing defect detection using the generalized synchrosqueezing transform guided by time-frequency ridge enhancement. *ISA Transactions*, 2016, 60(1): 274–284.
[12] P Tao, C Li, Y X Sheng, et al. A synchrosqueezing transform based method for rotor fault diagnosis of squirrel-cage induction motors. *Proceedings of the IEEE International Conference on Control*, Xi'an, China, July 26, 2013: 6261–6266.
[13] P Puche-Panadero, M Pineda-Sanchez, M Riera-Guasp, et al. Improved resolution of the MCSA method via Hilbert transform, enabling the diagnosis of rotor asymmetries at very low slip. *IEEE Transactions on Energy Conversion*, 2009, 24(1): 52–59.
[14] D F Piresa, V F Pires, J F Martins, et al. Rotor cage fault diagnosis in three-phase induction motors based on a current and virtual flux approach. *Energy Conversion & Management*, 2009, 50(4): 1026–1032.
[15] B Q Xu, L LSun. Concurrent discrimination of rotor fault and load oscillation in induction motors. *Proceedings of the CSEE*, 2016, 36(23): 6518–6527. (in Chinese)
[16] F Gu, T Wang, A Alwodai, et al. A new method of accurate broken rotor bar diagnosis based on modulation signal bispectrum analysis of motor current signals. *Mechanical Systems and Signal Processing*, 2014, 50(51): 400–413.
[17] Y H Kim, Y W Youn, D H Hwang, et al. High-resolution parameter estimation method to identify broken rotor bar faults in induction motors. *IEEE Transactions on Industrial Electronics*, 2013, 60(9): 4103–4117.
[18] B Q Xu, L LSun, H M Li. A detection method for rotor fault induction motors based on high frequency resolution spectrum estimation technique and optimization algorithm. *Proceedings of the CSEE*, 2013, 33(3): 140–147. (in Chinese)
[19] L P Shi, P P Wang, Y J Hu, et al. Broken rotor bar fault diagnosis of induction motors based on bare-bone particle swarm optimization and support vector machine. *Transactions of China Electrotechnical Society*, 2014, 29(1): 147–153. (in Chinese)
[20] X Wen, L Shao, Y Xue, et al. A rapid learning algorithm for vehicle classification. *Information Sciences*, 2015, 29(5): 395–406.
[21] B Gu, V S Sheng, Z Wang, et al. Incremental learning for v-support vector regression. *Neural Networks*, 2015, 67(7): 140–150.
[22] B Gu, V S Sheng, K Y Tay, et al. Incremental support vector learning for ordinal regression. *IEEE Transactions on Neural Networks & Learning Systems*, 2015, 26(7): 1403–1416.
[23] B Gu, X Sun, V S Sheng. Structural minimaxprobability machine. *IEEE Transactions on Neural Networks & Learning Systems*, 2016, 28(7): 1646–1656.
[24] Y Lin, H Zhao, H Ding. Solution of inverse kinematics for general robot manipulators based on multiple population genetic algorithm. *Journal of Mechanical Engineering*, 2017, 53(3): 1–8. (in Chinese)
[25] H W Tang, W Sun, W Y Zhang, et al. Wavelet neural network method based on particle swarm optimization for obstacle recognition of power line deicing robot. *Journal of Mechanical Engineering*, 2017, 53(13): 55–63. (in Chinese)
[26] J Kennedy, R C Eberhart. Particle swarm optimization. *Proceedings of the IEEE International Conference on Neural Networks*, Piscataway, New Jersey, USA, November 27–December 1, 1995: 1942–1948.
[27] J Kennedy. Bare bones particle swarms. *Proceedings of the IEEE International Conference on Swarm Intelligence Symposium*, Indiana, USA, April 26, 2003: 80–87.
[28] M J D Powell. On the global convergence of trust region algorithms for unconstrained optimization. *Mathematical Programming*, 1984, 29(3): 297–303.
[29] F J Solis, R J Wets. Minimization by random search techniques. *Mathematics of Operations Research*, 1981, 6(1): 19–30.